Original Research Article
Design of a Tri-Band Minkowski Fractal MIMO Antenna for FR2 5G Applications

ABSTRACT

The growing importance of fifth-generation (5G) communication technologies for the Internet-of-Things have made it necessary to design multi-element antennas that operate within the millimetre-wave spectrum. However, simultaneously achieving multiple operating frequencies, high gain and good isolation between the elements of such small-sized antennas is a challenging task. In this research, a composite right/left hand millimetre-wave fractal antenna was designed for 5G mobile terminals, in order to simultaneously satisfy these key design goals. This aim was accomplished by designing a 2 x 2 multiple-input, multiple output (MIMO) antenna based on the second-order Minkowski fractalusing an electromagneticssimulation software, Computer Simulation Technology (CST) Studio Suite ®. Two composite-right/left hand structures were included on the reverse side of the antenna, to reduce the coupling between the MIMO antenna elements. Simulation results show that the designed antenna operates at three frequency bands within the millimetre-wave spectrum, namely 25.52 GHz – 28.23 GHz, 36.5 GHz – 37.5 GHz, and 47.7 GHz – 49.7 GHz. The maximum antenna gains at these three bands are 6.9 dBi, 7.5 dBi, and 6.0 dBi, respectively. Also, good isolation is realized between the antenna elements at the operating frequencies, with a minimum value of 10.8 dB. With a spacing of 0.03λ between the MIMO antenna elements, the overall size of the designed antenna was 30 mm x 12 mm x 0.508 mm, which compares positively with other related fractal antenna designs. The designed antenna shows good prospects for integration into various mobile terminal devices to aid 5G-based millimetre-wave communications.

Keywords: 5G; FR2;millimeter-wave; MIMO antenna; Minkowski fractal; tri-band, IoT.

1. INTRODUCTION

The evolution of wireless mobile communication technology, from the first generation to the present fifth-generation (5G) technology, has been accompanied by notable innovations. The driving purpose for these advancements has been the desire to achieve wider coverage, increased data speeds, and improved connection reliability, while maximizing user experience. 5G wireless technology enables gigabyte wireless connectivity for devices. In the development of the required specifications, 5G is proposed as an enabler for new service applications such as smart factories, smart cities, smart homes, seamless connectivity between self-driving cars and telemedicine, to name a few. The three foremost scenarios for the application of 5G networks are enhanced Mobile BroadBand (eMBB) at 10 Gbps; ultra-reliable and low latency communication (URLLC), with less than 1 ms latency, and massive machine-type communication (mMTC) at a density of 1 million devices per kilometer. The mMTCusage scenario envisages that there will be a much increased diversity of mobile devices, beyond smartphones [1].

Multiple-input multiple-output (MIMO), massive-MIMO, and phased array antennas are the key driving antenna technologies for the 5G air-interface, which is also known as the 5G New Radio (NR) [1]. Based on the 5G NR categorization, there are two operating frequency ranges for 5G communication networks, namely the Frequency Range 1 (FR1) and Frequency Range 2 (FR2). FR1 frequencies are between 450 MHz to 6 GHz, while FR2 frequencies are in the

millimetre-wave (mm-wave) spectrum, spanning 24.25 GHz to 52.6 GHz [1]. The mm-wave bands have different propagation characteristics compared to the sub-6GHz bands. Specifically, the sub-6GHz bands have the characteristic of non-line-of-sight (NLOS) propagation. In contrast, the mm-wave bands provide shorter ranges with line-of-sight (LOS) propagation characteristics. These differences in propagation characteristics influence the design choices to be made when developing antennas to operate within these two frequency ranges.

Although FR2 mm-wave 5G is better suited for short-range, line-of-sight, high data-rate communication scenarios, there are some difficulties related to its use. One significant challenge is that the mm-wave signals are highly vulnerable to attenuation, and can be easily blocked by obstacles along the propagation path [2]. Also, the path loss at the mm-wave frequencies is significantly higher than sub-6GHz frequencies. Consequently, the antennas used at these frequencies should have high gains [3].Also, it is usually the case that the target communication devices where the antennas are integrated are required to simultaneously offer different services that are available in different frequency bands. This makes it desirable that the antennas employed in these devices should have good bandwidths and multi-band characteristics [3]. This would enable a single antenna serve for multiple applications, and reduce the overall count of antennas required for the devices. One of the key antenna design challenges for such devices is the limited available space for mounting them, especially when the mobile terminals are wearable or hand-held devices. So it is also necessary that a small size can be achieved without compromising the antenna's performance. Several studies have, therefore, focused on meeting the crucial antenna design goals of high gain, multi-band operation, and small size.

One notable technique for achieving high gain is through the use of multi-element antennas, and this has received significant research attention. For example, in [4] a 1 x 4 antenna array of four elliptical patch radiator elements is implemented on a Rogers RT/duroid 5880 substrate, and designed to resonate at 28 GHz and at 45 GHz. In this case, the maximum gain of the antenna is 7.6 dBi, and it occurs at 28 GHz. In another design, a 12 element antenna is implemented to operate between 27.06 GHz – 28.35 GHz [5]. The antenna achieves a peak gain of 16 dBi, which occurs at 28 GHz, and has a bandwidth of 1.29 GHz.MIMO antennas have also been designed to operate within the FR2 mm-wave band. An example of a MIMO design is found in [6], which is a MIMO antenna using four elements, achieving a 4.69 GHz bandwidth within the mm-wave 5G frequencies of 23.56 GHz –28.25 GHz. Another instance is a 4-port dual-band printed MIMO antenna array, which operates at two frequencies, namely 28 GHz and 38GHz. The design offers a high gain of about 7.9 dB at 28 GHz, and 13.7 dB at 37.3 GHz [7].

In order to realize multi-band operation, some of the common techniques used include the use of slots [8] and defected ground planes [9],Fractal antennas have also been designed to create multi-band response within the range of operating frequencies[10].One instance of a fractal antenna is a bow-tie-shaped irregular fractal antenna with a dual metasurface (DMS), which has been designed for directional radiation applications [11]. The antenna operates in two modes, namely at 2.39 GHz – 2.53 GHz, and at 2.88 GHz – 4.49 GHz. Also, square-shaped split-ring resonators arranged in a Sierpinski fractal pattern have been used to realize a dual-band antenna. The antenna operates at 1.75 GHz – 2.0 GHz, and at 3.01 GHz – 4.18 GHz, with maximum gains of 1.5 dBi and 2.05 dBi, respectively [9]. In another example, a Sierpinski triangle radiating element has been combined with a Hilbert curve ground plane structure to realize a fractal monopole MIMO antenna. The 2 x 2 MIMO antenna operates at three bands sub-6GHz 5G bands, namely, 2GHz - 3 GHz, 3.4GHz – 3.9 GHz, and 4.4GHz – 5.2 GHz [12].Other notable examples of fractal antennas designed for enhanced bandwidths include a second-order Minkowski fractal antenna for ultra-wideband applications [13] and a high-gain fractal antenna with broad bandwidth [14].

There has also been research that demonstrates how composite right/left hand (CRLH) structures can be combined with fractal antenna shapes, in order to enhance the performance of the antenna. It has also been demonstrated that coupling a CRLH structure to a Hilbert fractal array is able to improve both the gain and the bandwidth of the antenna. In one case, the realized antenna operates over two frequency bands, namely 3.3 GHz – 4.2 GHz, and 4.86 GHz – 5.98 GHz. The maximum antenna gains within these frequency bands were 7.24 dBi and 3.74 dBi, respectively [15]. In another example, a dual-band antenna is realized by the integration of a CRLH structure and the Hibert fractal, with the operating frequency bands being 3.72 GHz – 3.79 GHz, and 6.99 GHz – 8.55 GHz. The maximum antenna gains within these frequency bands were 5.28 dBi and 7.66 dBi, respectively. Another example of a CRLH structure and fractal combination is found in a CRLH-Minkowski fractal array antenna with 17 elements that has been designed with reconfigurable frequency characteristics [16]. This feature enables the antenna to be switched to operate over multiple frequency bands within the sub-6GHz 5G frequencies. Similarly, a CRLH structure has been combined with a Hilbert fractal ground plane structure, and a Sierpinski gasket fractal radiator in a 2 x 2 MIMO antenna with four elements, to provide increased isolation between the MIMO elements within the sub-6GHz 5G frequency range, while still achieving good bandwidth and bandwidth characteristics [12]. The realized antenna operates over three frequency bands, namely 2 GHz – 3 GHz, 3.4 GHz – 3.9 GHz, and 4.4 GHz – 5.2 GHz. The realized isolation between the antenna elements was 20 dB, while the maximum gain across the three operating frequency bands was 6.2 dBi.

Although the design of MIMO antennas using fractal shapes provides the advantage of achieving high gain and multi-band response, with a relatively simpler structure, there have not been many examples of the use of this approach to realize multi-band antennas for FR2 mm-wave 5G applications. This research gap forms the basis for the antenna design study in CST presented in this paper.Consequently, this paper presents a compact MIMO antenna design that employs fractal geometries to achieve multi-band characteristics and high-gain within the FR 2 mm-wave 5G frequencies. The rest of the paper is arranged as follows. The second section presents the methodology for the antenna design. The simulation results obtained in the study are provided and discussed in the third section of this paper. The last section presents a conclusion to the paper.

2. METHODOLOGY

2.1 Design of Initiator Square patch

A square-shaped radiator was used as the initiator shape for the Minkowski fractal. The square-shaped radiator was designed to provide resonance an initial single resonance frequency point within the mm-wave spectrum. A frequency of 28 GHz was arbitrarily chosen as this initial frequency point from which subsequent iterations in the design process were able to proceed. As is common with antenna designs at higher microwave frequencies, it is necessary that radiators are designed using good electrical conductors placed on dielectric substrate materials that have both low dielectric constants and dissipation factors. The substrate used is RT/duroid 5880, which has a dielectric constant ε_r = 2.2, and dissipation factor $\tan\delta$ = 0.0009.The required size of the square patch was derived from calculations using equations for the dimensions of a rectangular patch [17], which was designed to resonate at 28 GHz. The width of the rectangle, w was calculated using equation (1):

$$w = \frac{c}{2f_0\sqrt{\frac{\varepsilon_r+1}{2}}} \tag{1}$$

where f_0 = 28 GHz; c = 3 × 10^9m/s; and ε_r = 2.2.

The required length of the rectangle l was calculated using equation (2):

$$l = \frac{c}{2f_0\sqrt{\varepsilon_{eff}}} - 0.824h\left[\frac{(\varepsilon_{eff}+0.3)\left(\frac{w}{h}+0.264\right)}{(\varepsilon_{eff}-0.258)\left(\frac{w}{h}+0.8\right)}\right], \tag{2}$$

where h is the thickness of the substrate material, which is 0.508 mm. The effective permittivity ε_{eff} was calculated using equation (3):

$$\varepsilon_{eff} = \frac{\varepsilon_r+1}{2} + \frac{\varepsilon_r-1}{2}\left(\frac{1}{\sqrt{1+12\left(\frac{h}{w}\right)}}\right) \tag{3}$$

Using equations (1) – (3), the width and length of the rectangular patch were calculated as 4.232 mm and 3.279 mm, respectively. Since antenna size was one of the design considerations, the smaller dimension was chosen so that as the each side of the initiator initial square patch had a length l = 3.279 mm.

2.2 Design of Minkowski fractal patch

The mathematical approach for designing a Minkowski fractal, which is described in [18], was applied in this work.The Minkowski fractal was generated using the IFS described in equation (4):

$$V[A] = \mathrm{U}_{n=1}^{5}\, v_n(A) \tag{4}$$

where A is the square subset;

$V[A]$ is the Hutchinson operator, and is a transformation over the subset A;$v_n$is an affine linear transformation, which is defined as:

$$v_i(x', y') = \begin{pmatrix} r\cos\emptyset & s\sin\varphi \\ r\sin\emptyset & s\cos\varphi \end{pmatrix}\begin{pmatrix} x \\ y \end{pmatrix} + \begin{pmatrix} x_0 \\ y_0 \end{pmatrix} \tag{5}$$

where r and s are scaling factors, either >1 or <1. $\emptyset$ and φ are rotation angles, x and y, are Cartesian coordinates, x_0 and y_0 represent movement along the coordinate axes, and x' and y' are the final transformed coordinates.

For the Minkowski fractal shape, the rotation angles, $\emptyset = \varphi = 0$. The affine linear transformations in the first iteration were then defined as:

$$v_1(x', y') = \begin{pmatrix} \frac{2}{3} & 0 \\ 0 & \frac{2}{3} \end{pmatrix} \begin{pmatrix} x \\ y \end{pmatrix} \quad (6a)$$

$$v_2(x', y') = \begin{pmatrix} \frac{1}{3} & 0 \\ 0 & \frac{1}{3} \end{pmatrix} \begin{pmatrix} x \\ y \end{pmatrix} + \begin{pmatrix} \frac{1}{3} \\ \frac{1}{3} \end{pmatrix} \quad (6b)$$

$$v_3(x', y') = \begin{pmatrix} \frac{1}{3} & 0 \\ 0 & \frac{1}{3} \end{pmatrix} \begin{pmatrix} x \\ y \end{pmatrix} + \begin{pmatrix} \frac{1}{3} \\ -\frac{1}{3} \end{pmatrix} \quad (6c)$$

$$v_4(x', y') = \begin{pmatrix} \frac{1}{3} & 0 \\ 0 & \frac{1}{3} \end{pmatrix} \begin{pmatrix} x \\ y \end{pmatrix} + \begin{pmatrix} -\frac{1}{3} \\ \frac{1}{3} \end{pmatrix} \quad (6d)$$

$$v_5(x', y') = \begin{pmatrix} \frac{1}{3} & 0 \\ 0 & \frac{1}{3} \end{pmatrix} \begin{pmatrix} x \\ y \end{pmatrix} + \begin{pmatrix} -\frac{1}{3} \\ -\frac{1}{3} \end{pmatrix} \quad (6e)$$

Equations (5) and.(6a) – (6e), were used to model the first-order Minkowski fractal. The second-order Minkowski fractal was obtained by using transformations of the previous iteration, i.e:

$$A_n = V[A_{n-1}] \quad (7)$$

Figure 1 shows the evolution of the Minkowski fractal from the initiator square, through the first and second iterations. Using the computer simulator, CST Studio models of these iterations were designed using copper on RT/duriod 5880 substrate.

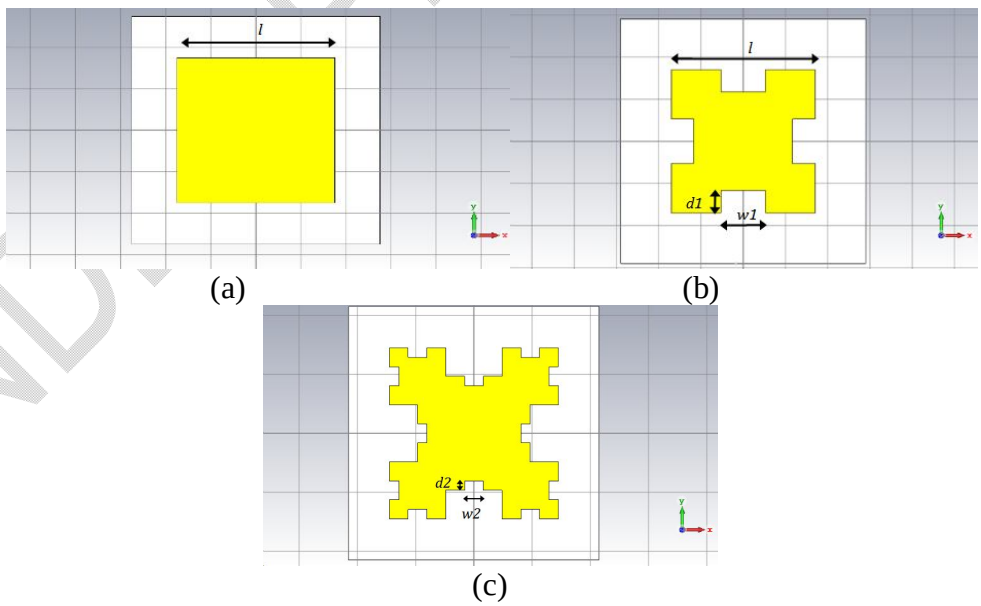

Fig 1. Iterations of Minkowski fractal radiator using copper on RT/duroid 5880 substrate: (a) Initiator square patch; (b) first-order fractal; (c) second-order fractal

A coplanar waveguide (CPW) was used as the feeding method to enable a signal input to the fractal radiator. This CPW method involved connecting a feed line to the fractal patch, which terminates at an edge of the dielectric substrate. To ensure that the feed line is straight, without corners or bends, and that it connects to a corner of the radiator, the Minkowski fractal was rotated 45^{o} along the z-axis. The antenna ground plane was placed on the same side of the antenna as the fractal patch, so that the reverse side of the dielectric substrate was left free for the implementation of the CRLH structure. The structure of a single second-order fractal antenna is shown in Figure 2.

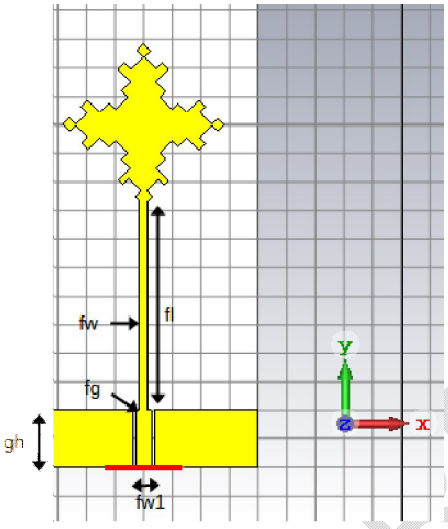

Fig. 2 Layout of second-order fractal antenna

2.3 Design of 2 x 2 MIMO antenna

The design of the four-element 2 x 2 MIMO antenna was based on duplicating the already modelled fractal antenna with a CPW feeding arrangement. To achieve this step, three geometrical transformations were carried out in the computer simulation software. The transformations are described as follows:

1. First, the single fractal antenna was duplicated, and the replica was placed side-by-side with the original antenna, along the x-axis, i.e. horizontally.

2. Next, the original antenna and its replica were jointly duplicated, and this joint duplicate was rotated 180o about the z-axis, so that it was upside down when compared to the original antenna and its replica.

3. Finally, the rotated duplicate antennas were moved along the y-axis so that their bottom edges coincided with the top edges of the combination of the original antenna and its first duplicate.

The layout of the 2 x 2 MIMO antenna can be seen in Figure 4(a).

2.4 Design of CRLH Structure

The length of the transmission line was chosen to correspond to the width of two antenna elements, placed side-by-side. To calculate the width of the transmission line, the line was approximated as a microstrip line of width *w* separated vertically from another conductor by a distance *h*.In this case, the second conductor is the antenna radiating element on the opposite side, while the separating distance is the thickness of the dielectric substrate. With this assumption made, the width of the transmission line was calculated using the transmission line solver macro in CST Studio, which implements the equation for calculating the width of a transmission line to obtain a specific characteristic impedance [19]:

$$w_l = \frac{8he^A}{e^{2A}-2}, \tag{8}$$

where

$$A = \frac{Z_0}{60}\sqrt{\frac{\varepsilon_r+1}{2}} + \frac{\varepsilon_r-1}{\varepsilon_r+1}\left(0.23 + \frac{0.11}{\varepsilon_r}\right) \tag{9}$$

Since the CRLH structure is intended to provide a high impedance across the frequency bands of interest in order to prevent mutual coupling between the antenna elements, a high characteristic impedance value Z_0 = 100 Ω was chosen, so that with ε_r = 2.2 and *h* = 0.508 mm for the RT/duroid 5880 dielectric substrate, the initial value of the transmission line

width was calculated as w_l = 0.45 mm. The microstrip transmission line provides the right-handed inductance and capacitance, i.e. series inductance and parallel capacitance, of the CRLH transmission line structure. The interdigital capacitor, was designed to have 5 fingers, and placed mid-way along the transmission line. Lastly, the width of the stub lines was chosen using the same assumptions made for the microstrip transmission line, so that their widths were calculated as 0.45 mm, to give a characteristic impedance of 100 Ω. The length of these lines was chosen to correspond with a quarter-wavelength ($\lambda/4$) at one of the resonance frequencies. The CRLH structure is shown in Figure 3 below:

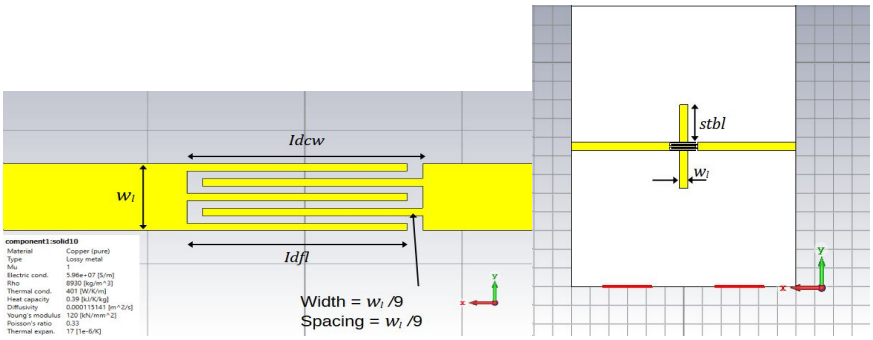

(a) Interdigital capacitor (b) microstrip line, stubs and interdigital capacitor

Fig3. CRLH structure

The overall layout of the antenna structure is shown in Figure 3, and the optimized dimensions are shown in Table 1.

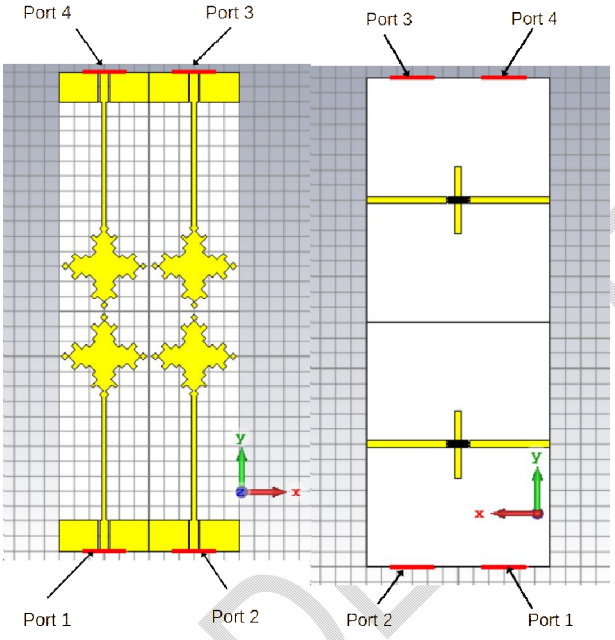

(a) Front view (b) Back view

Fig.4 Overall antenna layout

Table 1 Antenna Dimensions

Parameter	***L***	l_{sub}	***fl***	***fw***	***fw1***	***Fg***	***gh***	***Idcw***	***Idcfl***	w_l	***stbl***	***d1***	***d2***	***w1***	***w2***
Value (mm)	4	5	9	0.3	0.53	0.1	2	1.5	1.4	0.45	2	0.6	0.3	1.5	0.6

The antenna design was implemented using the Computer Simulation Technology (CST) Studio Suite ®. Various stages of the design process were modeled in the software, and simulations were run to observe the performance of the structure.

3. RESULTS AND DISCUSSION

Figure 5 shows the reflection coefficient of the initiator square patch (see Figure 1a) designed to resonate at 28 GHz. At the resonance frequency, the reflection coefficient has a value below -45 dB.

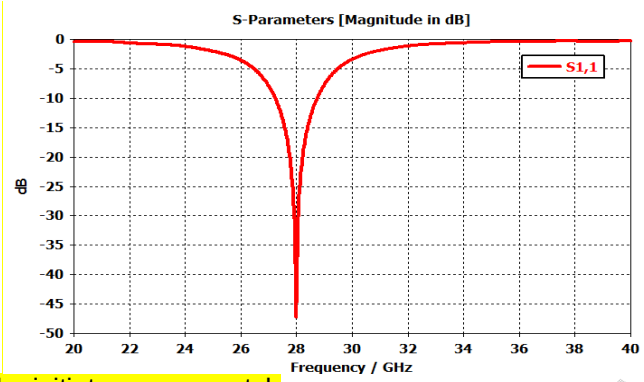

Fig. 5 Reflection coefficient of the initiator square patch

With this initiator square as the foundation, the iterative formulae were used to design the first-order Minkowski fractal shape (see Figure 1b). Figure 6 shows the reflection coefficient of the first-order Minkowski fractal antenna, with parametric studies carried out on its two cut dimensions, w1 and d1. First, the figure reveals the potential for a dual-band antenna using the first-order fractal. Also, the figure reveals that dimension w1 has a negligible impact on the reflection coefficient of the radiator. However, dimension d1 influences the depth and the frequencies at which the two resonances occur

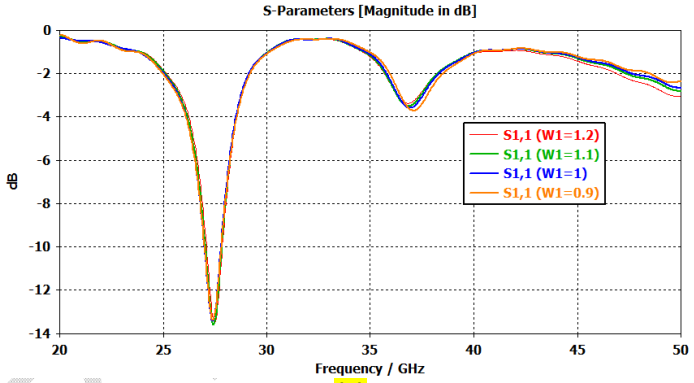

(a)

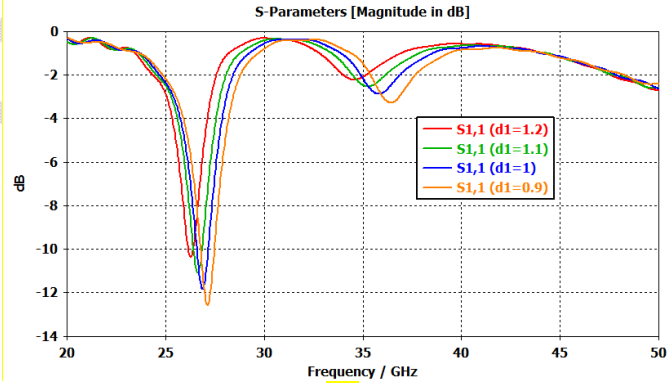

(b)

Fig 6 Reflection coefficient of first-order Minkowski fractal: (a) parametric study on dimension w1; (b) parametric study on dimension d1.

Next, a parametric study of dimensions of the CPW feed (see Figure 2) on the first-order Minkowski fractal structure is shown in Figure 7. From this figure it can be observed that the length of the feed line is the more significant dimension

that influences the frequencies at which both resonances can occur. In summary, these intermediate results on the first-order Minkowski fractal implied that one more resonance frequency could be achieved by increasing the order of the fractal to a second-order. Also, these results revealed the most important antenna dimensions to be optimized in order to provide good tri-band characteristics.

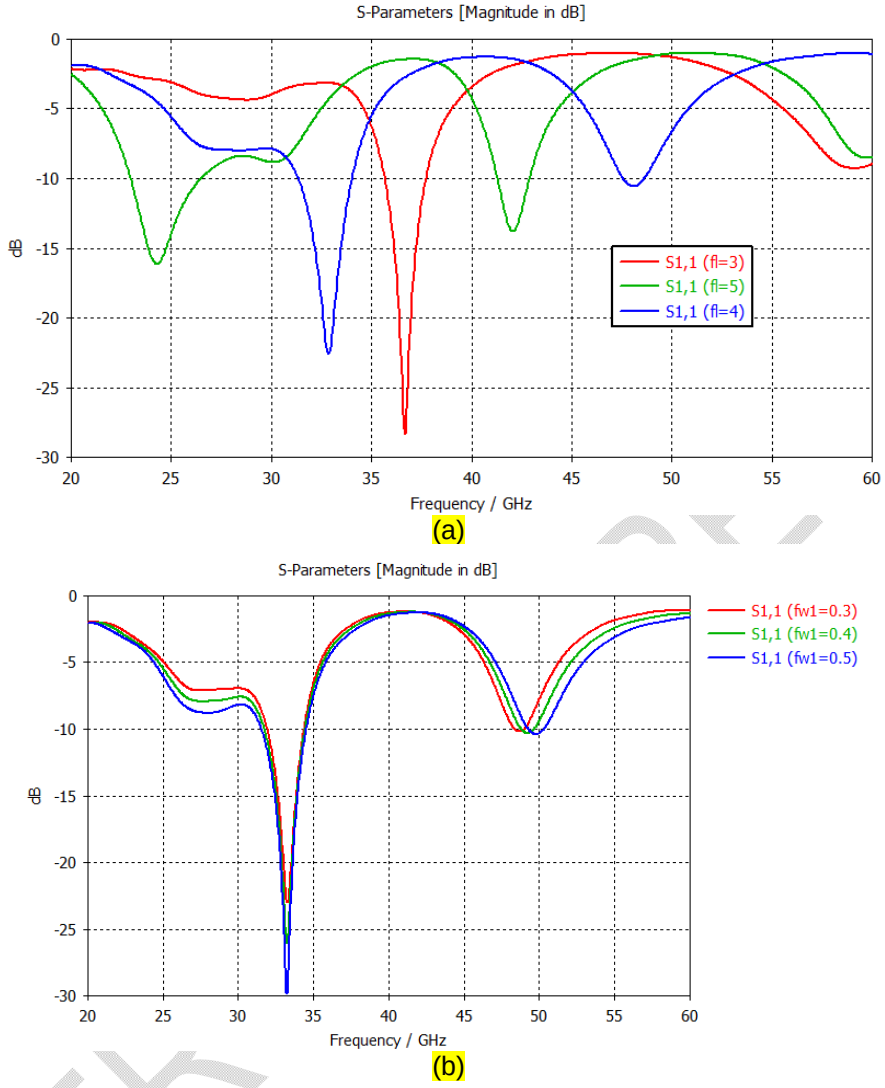

Fig. 7 Parametric study of CPW feed dimensions on first-order Minkowski fractal: (a) feed length (fl); (b) feed width (fw)

Based on the results obtained for a first-order fractal antenna, a second-order fractal antenna was designed, and the critical antenna dimensions were optimized.The reflection coefficient of the single second order fractal antenna is shown in Figure 8, which demonstrates that the fractal shape provides a tri-band frequency response, thereby meeting the goal of multi-band antenna operation.

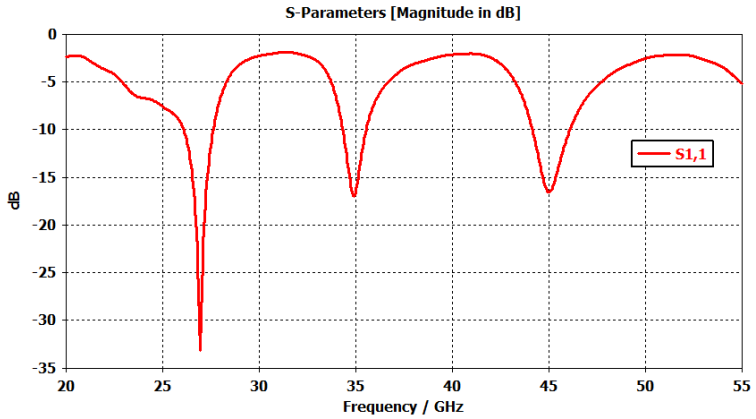

Fig. 8 Reflection coefficient of single second-order Minkowski fractal

Subsequently, a 4-element MIMO antenna, using the second-order Minkowski fractal shape was designed. The reflection and transmission coefficients of the 2 x 2 MIMO fractal antenna, without the CRLH structure, is shown in Figure 9.

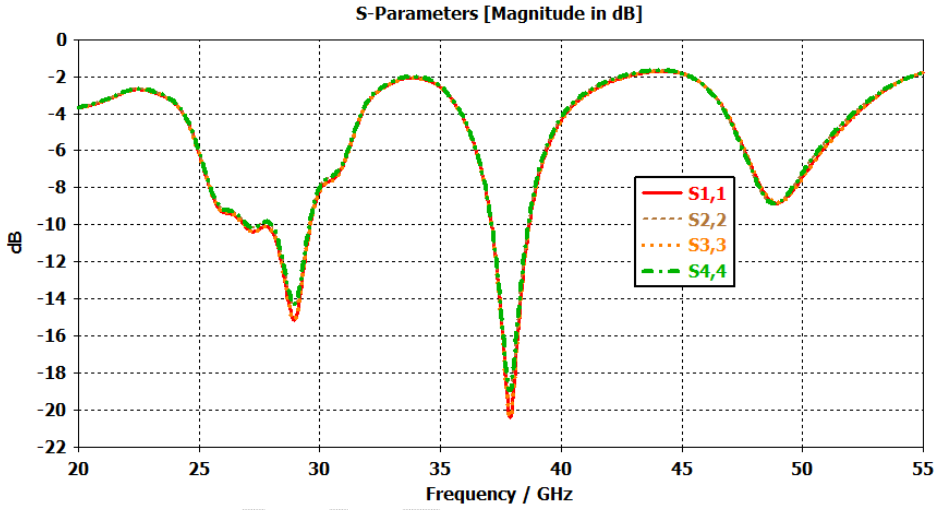

(a) Reflection coefficients

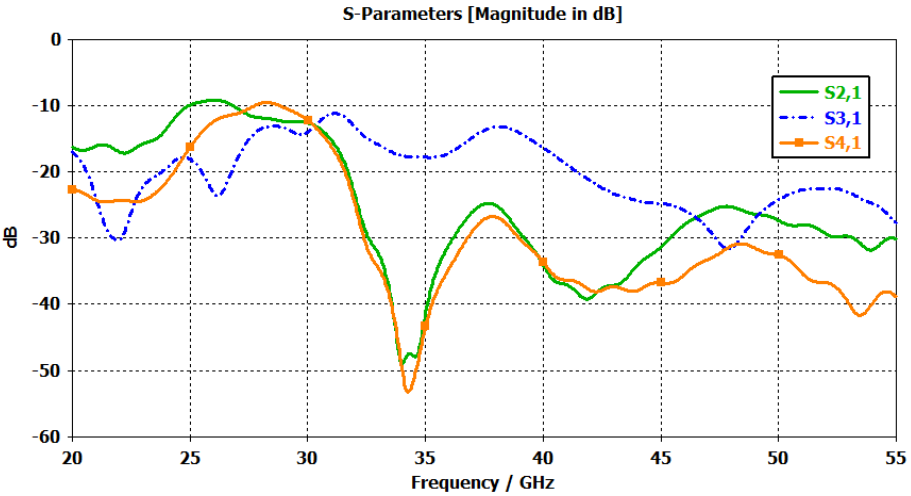

(b) Transmission coefficients

Fig. 9. S-parameters of 2 x 2 MIMO antenna without CRLH structure

The Figure shows that due to the close spacing between the antenna elements, the highest resonant frequency has been lost, while the isolation between the antennas is less than 10 dB between 25 GHz and 30 GHz. With the inclusion of the CRLH structure on the reverse side of the antenna (see Figure 4), the reflection and transmission coefficients are modified as shown in Figure 10.

Figure 10 demonstrates that the CRLH structure restores the 3 resonant frequencies, and also increases the isolation between the antenna elements, between 25 GHz and 30 GHz. With the CRLH structure in place, the operating bands of the antenna are as follows:

1. Band 1: 25.52 GHz – 28.23 GHz. Impedance bandwidth: 2.71 GHz
2. Band 2: 36.5 GHz – 37.5 GHz. Impedance bandwidth: 1 GHz
3. Band 3: 47.7 GHz – 49.7 GHz. Impedance bandwidth: 2 GHz

The corresponding minimum isolation values are band 1: 10.8 dB; band 2: 15 dB; and band 3: 26.5 dB.The radiation patterns of the antenna are shown in Figure 11

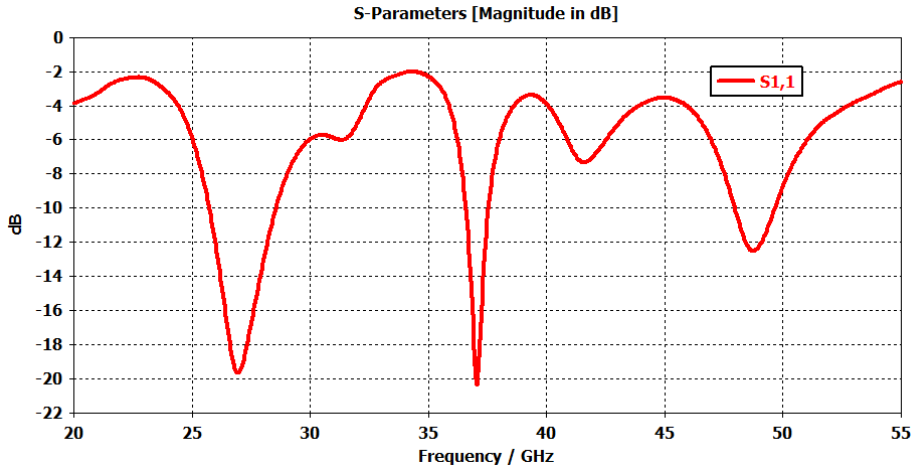

(a) Reflection coefficient

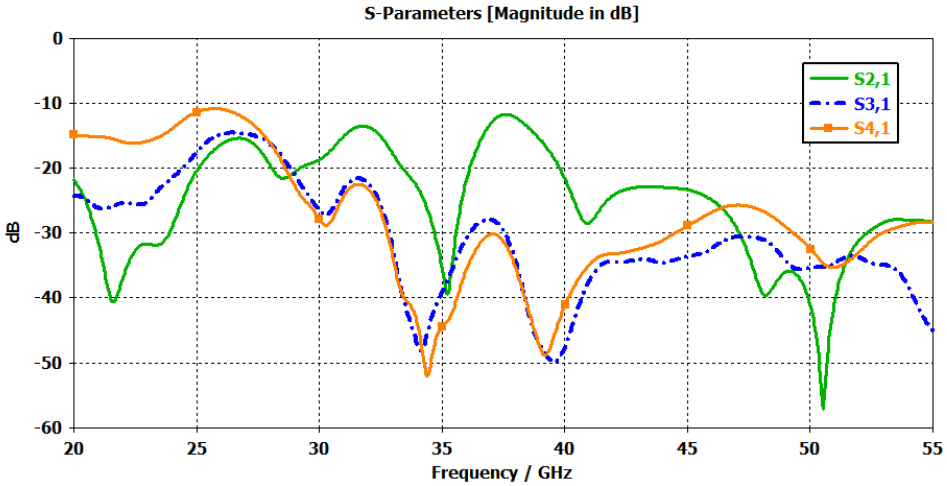

(a) Transmission coefficient

Fig. 10. S-parameter of 2 x 2 MIMO antenna with CRLH structure

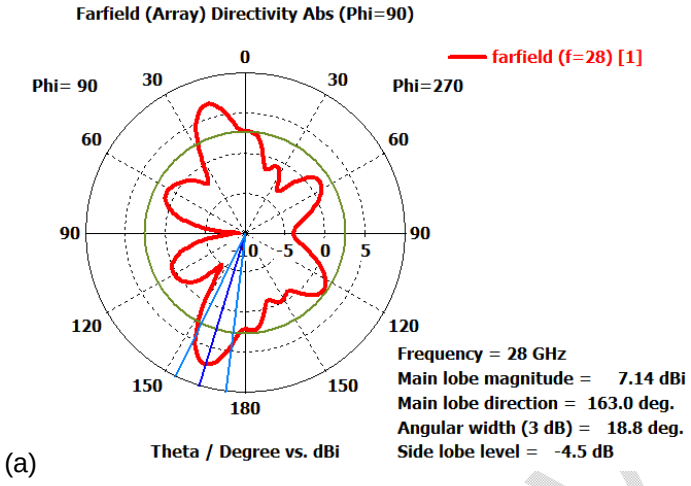

(a)

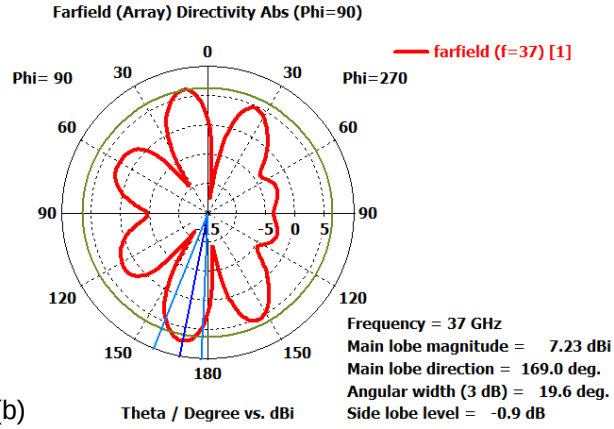

(b)

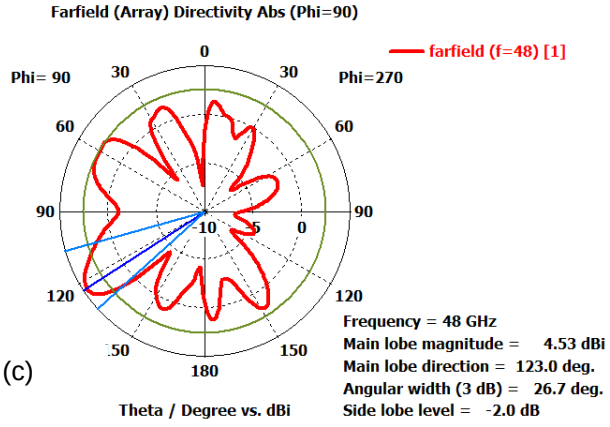

(c)

Fig. 11 Radiation patterns of 2 x 2 Minkowski fractal MIMO antenna with CRLH at resonance frequencies: (a) 28 GHz, (b) 37 GHz, (c) 48 GHz

The maximum antenna gains within these three bands are shown in Figure 12. The maximum gains of 6.9 dB, 7.5 dB and 6.0 dB were achieved in Bands 1, 2 and 3, respectively.

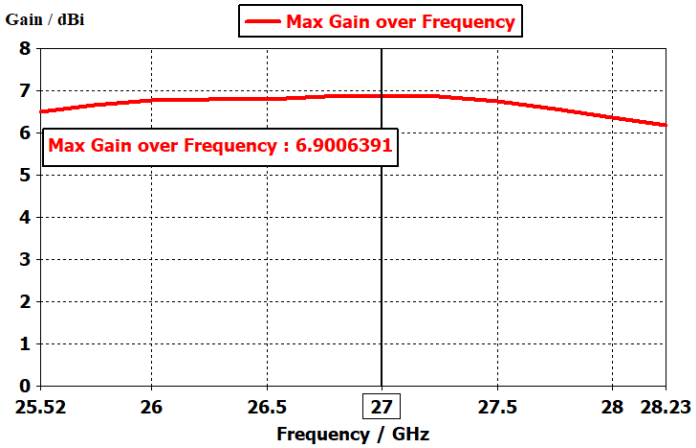

(a) Band 1

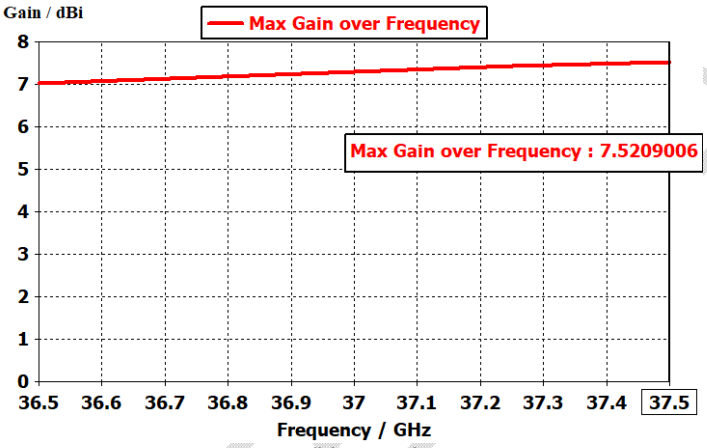

(b) Band 2

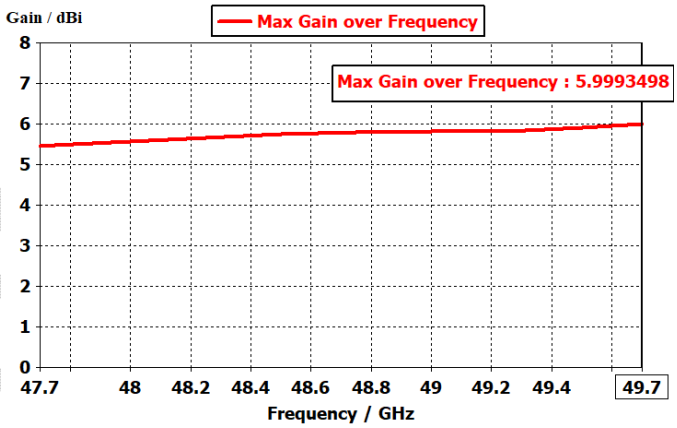

(c) Band 3

Fig. 12 Maximum gain over frequency within the three resonance bands

The MIMO antenna parameters of envelope correlation coefficient (ECC) and Diversity Gain (DG) were calculated based on equations (10) and (11)[12]:

$$ECC = \frac{\left|\iint_{4\pi}\left[\overrightarrow{F_1}(\theta,\varphi)*\overrightarrow{F_2}(\theta,\varphi)\right]d\Omega\right|}{\iint_{4\pi}\left[\overrightarrow{F_1}(\theta,\varphi)\right]^2 d\Omega \iint_{4\pi}\left[\overrightarrow{F_2}(\theta,\varphi)\right]^2 d\Omega} \quad (10)$$

$$DG = 10\sqrt{1-ECC} \quad (11)$$

Where, $\overrightarrow{F_1}(\theta,\varphi)$and $\overrightarrow{F_2}(\theta,\varphi)$ are the radiation patterns caused by signal inputs at the first port and the second port, measured over the horizontal and vertical angles $\theta$and φ. Ω is the 3D angle over which the radiation pattern is plotted.

These parameters are plotted in Figure 13. The Figure shows that the antenna meets the ECC threshold value of <0.5 at the three operating frequency bands, and also meets the DG threshold value of 10 dB at these frequency bands.

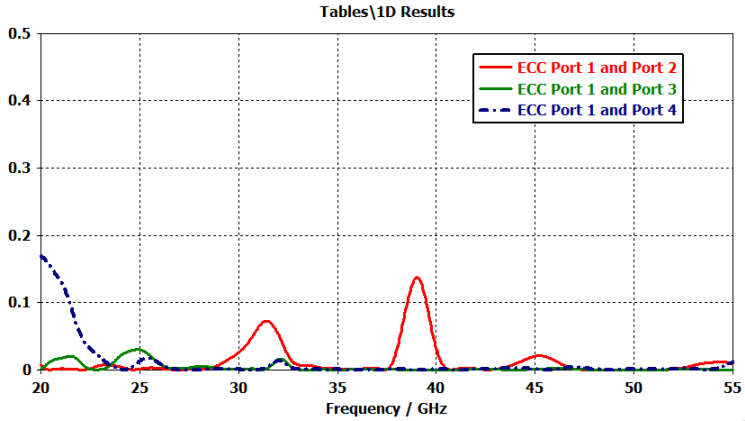

(a) Envelope Correlation Coefficient (ECC) between antenna ports

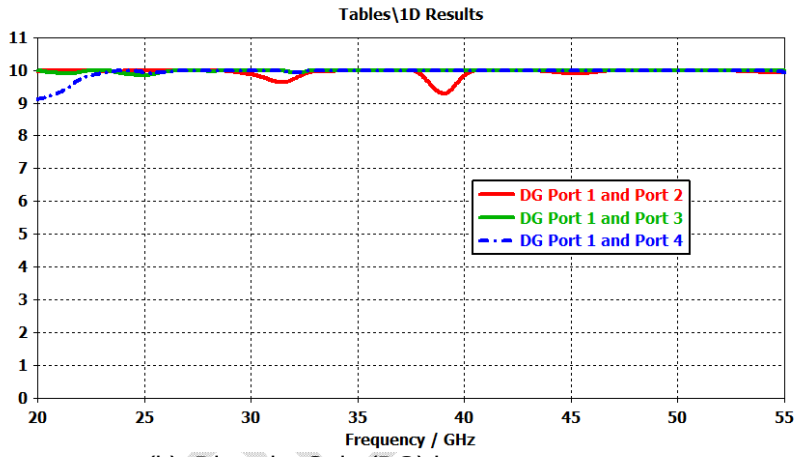

(b) Diversity Gain (DG) between antenna ports

Fig. 13 MIMO antenna parameters

In summary, the performance of the designed antenna is presented in Table 2 below:

Table 2 Summary of simulation results

Band	Resonant Frequency (GHz)	Bandwidth (GHz)	Max Gain (dBi)	Minimum Coupling Loss (dB)	Minimum Isolation (dB)	Radiation Efficiency (%)	Maximum ECC	Maximum Diversity Gain (dB)
Band 1	28	2.71	6.9	-22.5	10.8	91	0.005	10
Band 2	37	1	7.5	-38.1	15	91	0.02	10
Band 3	48	2	6	-40.	26.5	94	0.0001	10

In Table 3 the performance of the final antenna design is compared with the most closely related designs, which design fractal antennas with CRLH inclusions. Compared to other works, this work was able to achieve three frequency bands, and the minimum gain achieved by this antenna was higher than the minimum provided by other multi-band fractal antenna designs. In addition, the isolation of more than 10 dB was achieved using a much smaller inter-element spacing than is found in other fractal antenna designs. Therefore, the antenna designed in this work compares favourably with other designs of CRLH fractal antennas provided in the literature.

Table 3 Performance of 2 x 2 Minkowski fractal antenna compared with similar fractal designs for 5G applications

Reference	No. of frequency bands	Gains	5G Band	Isolation	Inter-element spacing
[20]	2 bands	5.28 dBi and 7.66 dBi	FR1	-	5.1 mm
[15]	2 bands	7.24dBi and 3.74dBi	FR1	-	6.1 mm
[12]	3 bands	6.2 dBi, ~5 dBi and ~5 dBi	FR1	> 20 dBi	1 mm
This research	3 bands	6.9 dBi, 7.5 dBi and 6 dBi	FR2	> 10 dBi	0.34 mm

4. CONCLUSION

This paper has demonstrated the use of a Minkowski fractal shape as the radiating element in a planar antenna in order to achieve multiple resonant frequency bands. A second-order Minkowski fractal antenna has been designed in an electromagnetics simulation software, CST Studio Suite ®, to obtain three resonant frequency bands within the FR2 band of frequencies designated for mm-wave 5G. By implementing a 2 x 2 MIMO configuration using four of these fractal elements, in addition to a CRLH structure behind the antennas, the design achieves high gains and isolation across the resonant frequency bands.

Simulation results show that the designed antenna was able to achieve three frequency bands of operation, namely 25.52 GHz – 28.23 GHz, 36.5 GHz – 37.5 GHz, and 47.7 GHz – 49.7 GHz. The maximum gains within these three bands were 6.9 dBi, 7.5 dBi, and 6.0 dBi. Lastly, the minimum isolation between the antenna elements across the full range of FR2 frequencies was 10.8 dB, which is greater than the threshold value of 10 dB. The realized antenna has dimensions of 30 mm x 12 mm x 0.508 mm, which is small enough to be embedded in various mobile devices to aid 5G-enabled machine-to-machine communications.

Disclaimer (Artificial intelligence)

Authors hereby declare that NO generative AI technologies such as Large Language Models (ChatGPT, COPILOT, etc) and text-to-image generators have been used during writing or editing of manuscripts.

REFERENCES

[1] M. Pant and L. Malviya, “Design, developments, and applications of 5G antennas: a review,” *Int. J. Microw. Wirel. Technol.*, vol. 15, no. 1, pp. 156–182, Feb. 2023, doi: 10.1017/S1759078722000095.

[2] P. Tiwari, V. Gahlaut, M. Kaushik, P. Rani, A. Shastri, and B. Singh, “Advancing 5G Connectivity: A Comprehensive Review of MIMO Antennas for 5G Applications,” *Int. J. Antennas Propag.*, vol. 2023, pp. 1–19, Aug. 2023, doi: 10.1155/2023/5906721.

[3] M. Ikram, K. Sultan, M. F. Lateef, and A. S. M. Alqadami, “A Road towards 6G Communication—A Review of 5G Antennas, Arrays, and Wearable Devices,” *Electronics*, vol. 11, no. 1, p. 169, Jan. 2022, doi: 10.3390/electronics11010169.

[4] M. I. Khattak, A. Sohail, U. Khan, Z. Barki, and G. Witjaksono, “Elliptical Slot Circular Patch Antenna Array with Dual Band Behaviour for Future 5G Mobile Communication Networks,” *Prog. Electromagn. Res. C*, vol. 89, pp. 133–147, 2019, doi: 10.2528/PIERC18101401.

[5] L. Malviya and P. Gupta, “Millimeter Wave High-Gain Antenna Array for Wireless Applications,” *IETE J. Res.*, vol. 69, no. 5, pp. 2645–2654, Jul. 2023, doi: 10.1080/03772063.2021.1903346.

[6] R. K. Mistri, A. K. Singh, S. K. Mahto, and R. Sinha, “Quad element millimetre-wave MIMO antenna for 5G communication,” *J. Electromagn. Waves Appl.*, vol. 37, no. 15, pp. 1258–1273, 2023.

[7] B. Aghoutane, S. Das, M. E. Ghzaoui, B. Madhav, and H. El Faylali, “A novel dual band high gain 4-port millimeter wave MIMO antenna array for 28/37 GHz 5G applications,” *AEU-Int. J. Electron. Commun.*, vol. 145, p. 154071, 2022.

[8] I. Ishteyaq, I. Shah Masoodi, and K. Muzaffar, “A compact double-band planar printed slot antenna for sub-6 GHz 5G wireless applications,” *Int. J. Microw. Wirel. Technol.*, vol. 13, no. 5, pp. 469–477, Jun. 2021, doi: 10.1017/S1759078720001269.

[9] U. Patel, T. Upadhyaya, A. Desai, R. Pandey, and K. Pandya, “Dual-band compact split-ring resonator-shaped fractal antenna with defected ground plane for sub-6-GHz 5G and global system for mobile communication applications,” *Int. J. Commun. Syst.*, vol. 35, no. 7, p. e5105, 2022.
[10] K. S. Vupputuri, S. Kamani, S. A. Sale, Y. R. Reddy, and J. P. Sudabathula, “Design and Analysis of Fractal Antenna for Wireless Communications,” in *2023 7th International Conference on Computing Methodologies and Communication (ICCMC)*, IEEE, 2023, pp. 1–5.
[11] A. Mohanty, B. R. Behera, K. P. Esselle, M. H. Alsharif, A. Jahid, and S. A. H. Mohsan, “Investigation of a dual-layer metasurface-inspired fractal antenna with dual-polarized/-modes for 4G/5G applications,” *Electronics*, vol. 11, no. 15, p. 2371, 2022.
[12] S. H. Ghadeer *et al.*, “An innovative fractal monopole MIMO antenna for modern 5G applications,” *AEU - Int. J. Electron. Commun.*, vol. 159, p. 154480, Feb. 2023, doi: 10.1016/j.aeue.2022.154480.
[13] E. Joseph, P. Kumar, and T. Afullo, “Design and Performance Evaluation of a Second-Order Iterated Circular Minkowski Fractal Antenna for Ultra-Wideband Applications,” *Fractal Fract.*, vol. 7, no. 11, p. 806, Nov. 2023, doi: 10.3390/fractalfract7110806.
[14] S. K. Patel and A. Baz, “O-Shape Fractal Antenna Optimized Design with Broad Bandwidth and High Gain for 6G Mobile Communication Devices,” *Fractal Fract.*, vol. 8, no. 1, p. 17, Dec. 2023, doi: 10.3390/fractalfract8010017.
[15] M. M. Ismail, T. A. Elwi, and A. J. Salim, “A Miniaturized Printed Circuit CRLH Antenna-based Hilbert Metamaterial Array,” *J. Commun. Softw. Syst.*, vol. 18, no. 3, pp. 236–243, 2022, doi: 10.24138/jcomss-2022-0030.
[16] M. M. Ismail, T. A. Elwi, and A. J. Salim, “Reconfigurable Composite Right/Left-Handed Transmission Line Antenna Based Minkowski- Stepped Impedance Resonator Structure For 5G Communication Networks,” vol. 18, 2023.
[17] C. A. Balanis, *Antenna theory: analysis and design*. John wiley & sons, 2016.
[18] Anguera *et al.*, “Fractal Antennas: An Historical Perspective,” *Fractal Fract.*, vol. 4, no. 1, p. 3, Jan. 2020, doi: 10.3390/fractalfract4010003.
[19] D. M. Pozar, *Microwave engineering: theory and techniques*. John wiley & sons, 2021.
[20] M. Ismail, T. Elwi, and A. Salim, “Antenna Gain-Bandwidth Enhancements Using CRLH Hilbert Fractal-based Structure,” *Eng. Technol. J.*, vol. 41, no. 2, pp. 1–10, Dec. 2022, doi: 10.30684/etj.2022.132987.1160.